Analysis Note:

Measurement of Ξ production in Au+Au collisions at $\sqrt{s_{NN}} = 3$ GeV

Yingjie Zhou, Guannan Xie, Yaping Wang

Abstract

In this note, we present the first measurement of Ξ^- hyperon production as well as the ϕ/Ξ^- ratio in Au+Au collisions at $\sqrt{s_{NN}} = 3$ GeV with the STAR experiment under its fixed target configuration at RHIC. Ξ^- is measured through its hadronic decay channels, $\Xi^- \rightarrow \Lambda(p\pi^-) + \pi^-$. The transverse momentum (p_T) spectra of Ξ^- is presented in different centrality and rapidity intervals. The total production yields and the ratios within a 4π acceptance window are calculated and compared to thermal model predictions. The grand canonical ensemble (GCE) calculation shows a clear discrepancy from our measurement.

CONTENTS

1. BASIC INFORMATION

The bad run list, event selection, centrality definition are identical to the ones used for ϕ-meson analysis. We refer to the ϕ-meson analysis section for details.

The $\bar{\Xi}^+$ statistic is very small in this dataset, we only reporet Ξ^- result.

The analysis is similar as ϕ-meson analysis, here is the summary of analysis procedure.

We firstly get Ξ^- counts in centrality/rapidity/p_T bins from data, the number of Ξ^- is extracted using a simple bin counting method. To get real invariant mass spectrum of Ξ^- within STAR acceptance, the raw spectrum should correct for the efficiency. The efficiency is calculated in p_T-rapidity bins from embedding. We know efficiency depends on the p_T spectrum and rapidity distribution of the input simulation, our embedding input is flat p_T and η distribution, and the p_T-rapidity distribution of Ξ^- at 3 GeV is not well known. So currently what we did is to using efficiency from flat p_T and η embedding sample to get realistic dN/dp_T and dN/dy distributions to weight the embedding simulation. Then using weighted embedding sample to get efficiency, correct for efficiency for p_T spectra in rapidity slices. Since our measurements can only achieve some certain momentum and rapidity range, we need to rely on functions to extrapolate to unmeasured range, for both dN/dp_T down to 0 p_T and $dNdy$ go to 4π acceptance ($y = [-2, 2]$) window.

2. Ξ^- RECONSTRUCTION

The Ξ^- are reconstructed via the hadronic decay channel $\Xi^- \rightarrow \Lambda + \pi^-$ with a branching ratio (B.R.) of 99.9% and $\Lambda \rightarrow p + \pi^-$ with a branching ratio (B.R.) of 63.9%. For particle identification of pions and protons, we use $|n\sigma_{p/\pi}| < 3$. If TOF information is available, we will add cuts: $-0.06 < m_\pi^2 < 0.1, 0.5 < m_p^2 < 1.5$.

Fig. **??** shows TOF m^2 information versus momentum achieved from Run18 Au+Au 3GeV, there are several clear bands for different particle species such as π, k, p, also the red dash line indicate the cut that we applied.

We are using the KFParticle package to reconstruct Ξ^-. The cuts used for the analysis are listed in Tab. **??**.

Fig. **??** show the invariant mass distribution for $\Lambda - \pi^-$ pairs in the p_T region of 0.5-2.0 GeV/c for 0-40% central collisions. We will take this plot to show how we extract the Ξ^- counts. For all the p_T-rapidity bins invariant mass spectrum fit can be found in the appendix **??**.

FIG. 1. TOF m^2 versus momentum achieved from Run18 Au+Au 3GeV.

TABLE I. Tracks and topological cuts for Ξ^- analysis.

nHitsFit>=15
$\chi^2_{topo} < 10$
$\chi^2_{NDF} < 10$
Ξ^- decay length $< \Lambda(\leftarrow \Xi)$ decay length
$LdL_{\Xi^-} > 6$
$DCA_{\Lambda-\pi} < 0.8$ cm
$DCA_{p-\pi^-_{\text{bach}}} < 0.8$ cm
$\chi^2_{prim} > 10$

FIG. 2. Signal and background invariant mass distribution for $\Lambda - \pi^-$ pairs the p_{T} region of 0.5-2.0 GeV/c for 0-40% central collisions, shown in black point. Rotation background, residual background are shown in blue open circle and blue dash line, respectively. The final background subtracted $\Lambda - \pi^-$ pairs is shown in red line, the counting window is indicated as the vertical red dash lines.

To obtain the number of Ξ^- signal, we are subtracting the background from raw counts after applying those cuts (Tab. **??**). In our analysis we are using rotation background, which is rotating the bachelor π^- tracks by a random degree in 150 to 210 degree then reconstruct Ξ^- by $\Lambda - \pi^-$ pair. In order to decrease the fluctuations and statistical uncertainty from this rotation background,

4

we generated 20 times of total number of event, so we at the end need to scaled it back into the correct number of event. The normalization is using the side band region $(1.30, 1.31)$ and $(1.34, 1.35)\text{GeV/c}^2$. The data and the background are shown in Fig. **??** in black solid and blue open circle. The background is subsequently subtracted from the data which is shown in blue line. One can see that the background is well described by the rotation method. In case there is any residual background we fit the remaining Ξ^- distribution with Gaussian + linear function, the linear function (blue dash line) is to take care of the residual background. The signal Ξ^- is shown in red line, the fit region is $(1.31, 1.35)\text{GeV/c}^2$. We extract the background counts (pol1) inside $|m - m_{\text{PDG}}| < 3\sigma$ window, where the σ is from the $0 - 60\%$ invariant mass fit and it's fixed in the fitting procedure and are indicated as the two vertical red dash lines in Fig. **??**. Bin counting method is used to extract counts in peak region, signal counts = data - bkg counts(linear function integrated in 3σ window). The statistics error was propagate from the fitting.
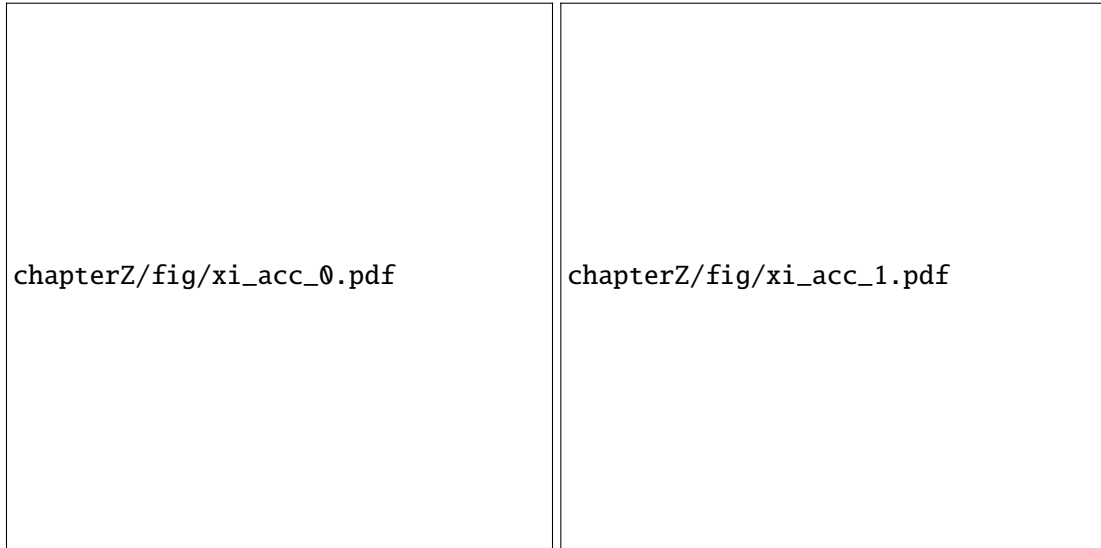

FIG. 3. Acceptance of Ξ^- for $0 - 10\%$(left) and $10 - 40\%$(right) centrality at $\sqrt{s_{NN}} = 3$ GeV.

Fig. **??** shows schematically the number of counts as a function of rapidity and transverse momentum in $0 - 10\%$ and $10 - 40\%$ centrality. To make sure each bin has a significance > 2, acceptance is divided into 4 rapidity bins, and for each rapidity bins, there are 3 or 4 p_{T} bins.

5

FIG. 4. Reconstruction efficiency of Ξ^-, as a function of y and p_T for $0-10\%$(left) and $10-40\%$(right) centrality at $\sqrt{s_{NN}} = 3$ GeV.

3. EFFICIENCY CORRECTION

The kinematic regions listed in the previous section does not have uniform efficiency, hence we need to apply efficiency correction. To calculate the efficiency, we reconstruct Ξ^- from embedding samples. The efficiency is obtained by dividing the number of reconstructed Ξ^- by the number of input Ξ^-, for each y and p_T bin. The track and topological cuts used are identical to the ones used in the data analysis (the cuts listed in Tab. **??**) except we don't apply TOF and TPC cut. The 2D efficiency is shown in Fig. **??**.

In our analysis, we don't do the TPC and TOF cut efficiency correction, and the efficiency effect should be small since we only have applied a very loose TPC and TOF cut. As can be seen from Fig. **??** TOF m^2 distributions, the PID cut is very loose, the PID efficiency should be about 1. And for the TPC $n\sigma$ cut efficiency, we firstly use a tight m^2 cut to select the samples, then like in ϕ-meson analysis assuming they follow the Gaussian function and get the mean value and sigma value as plotted in Fig. **??** upper two plots, and bottom plot shows the corresponding TPC $n\sigma$ cut efficiency for both kaon and pions, the efficiency is around 1.

To ensure the efficiency obtained is reliable, we compared the topological variables from data, and embedding. The cuts used will be varied as an estimate of the systematic uncertainties associated to efficiency corrections. It was confirmed that the topological variables can be reasonably described by the embedding (https://drupal.star.bnl.gov/STAR/system/files/210407_3GeV_Xiv1_pwg.pdf). For example, Fig. **??** show the χ^2 primary of p/π, Ξ^- decayed $\Lambda - \pi$ DCA and Λ decayed $p - \pi$ DCA distribution's comparision between data(black point) and embedding(red line). We can see the embedding is well consistent with data.

The cuts used will be varied as an estimate of the systematic uncertainties associated to efficiency corrections.

With those unweighted efficiency, we correct for data dN/dp_T spectrum to get a realistic Ξ^- dN/dp_T spectrum and dN/dy distributions. We taking p_T spectrum in $y[-0.8, 0]$ range, fitting with m_T exponential function with fit option "I", take the fit function as our real data p_T spectrum, showing Fig. **??** upper plot the cyan line. The middle plots are the m_T spectrum and the fit line is

FIG. 5. nσ_π, nσ_p mean, sigma and efficiency along with momentum p in Run18 Au+Au collisions at 3 GeV.

using the fit parameters from upper plots. To get dN vs. y distribution, we using 4 rapidity bins [-0.8, -0.6], [-0.6, -0.4],[-0.4, -0.2],[-0.2, 0], shown if upper plots in different color. For the integral yield, we rely on m_T exponential functions to extrapolate to unmeasured p_T region. The rapidity distributions is displayed in bottom plots. The full symbols show the measured data, while the open ones are data reflected with respect to $y = 0$ in the center-of-mass frame. Solid lines depict Gaussian function fits to the data points and are used to extrapolate to the unmeasured rapidity region. In the fitting procedure, the center of the Gaussian was fixed at zero to take into account the symmetry of the reaction.

Now we use the m_T exponential function from $y[-0.8, 0]$ for the input p_T, Gaussian function for the input rapidity, weight to both the MC generated and reconstructed Ξ^- 2D acceptance. Divide number of reconstructed counts by input MC counts to obtain efficiency. Fig. **??** show the reconstruction efficiency before and after weighting, for each p_T-rapidity bins. The open marker is from flat embedding sample, solid point is after efficiency correction. We can see a clear difference

7

⁹⁰ after efficiency correction on wider p_T bins.

4. SYSTEMATIC UNCERTAINTIES

⁹² We estimate systematic uncertainties in: efficiency corrections, and raw yield extraction. For
⁹³ raw yield extraction, we vary the signal fitting range. For efficiency corrections, we vary topo-
⁹⁴ logical cuts and nHitsFit cut. The details are summarized in Tab. **??**. For multiple variations of
⁹⁵ a variables, the maximum difference compare to the default one is taken as the systematic uncer-
⁹⁶ tainties source.

⁹⁷ For the integral yield, one important uncertainties coming from the extrapolation to the un-
⁹⁸ measured region. The default function formula is m_T exponential and different functional formula
⁹⁹ include the levy function, the blast-wave function, first order p_T exponential function are also be
¹⁰⁰ used, and the maximum difference compare to the default one is taken as the systematic uncertain-
¹⁰¹ ties source.

¹⁰² The final systematic error is to add all systematic source in quadrature.

¹⁰³ Fig. **??** show the weighted efficiency corrected m_T distributions for several rapidity bins, the
¹⁰⁴ different markers represent results from different cuts as list in the legend. As we can see, most of
¹⁰⁵ the data points are grouped together. For the systematic uncertainties, the contributions varied by
¹⁰⁶ p_T and rapidity bins, Tab. **??** lists the relative systematic uncertainty contribution from different
¹⁰⁷ cut in each rapidity bin for the $0 - 10\%$ and $10 - 40\%$ centrality.

¹⁰⁸ The default function formula is m_T exponential, we have different functional formula include
¹⁰⁹ the levy function, the blast-wave function, first order p_T exponential function. Fig. **??** shows the
¹¹⁰ dN/dp_T distributions for several rapidity bins for 0-10% and 10-40% centrality, the lines represent
¹¹¹ different functions as list in the legend. As can see, all four functions can describe the measured
¹¹² data reasonable well, even though they have some difference at low p_T which limited by the data
¹¹³ precision. The default function used for the extrapolation to the unmeasured range is the exponen-
¹¹⁴ tial function, while the others are quoted as the systematic uncertainties. On each plot, we list the
¹¹⁵ integral yield, as can see the difference can vary as large as 12-19% for $0 - 10\%$ centrality and
¹¹⁶ 13-16% for $10 - 40\%$ centrality.

¹¹⁷ Fig. **??** shows the Ξ^- dN/dy distributions for 0-10% and 10-40% centrality, the line show the
¹¹⁸ statistic uncertainty and the bracket shows the total systematic uncertainty include uncertainties
¹¹⁹ from extrapolation and topological cuts, raw yield extraction. Tab. **??** lists the relative systematic

TABLE II. Tracks and topological cuts for Ξ^- systematic uncertainty analysis. The bracketed values are the default selection, and the other values are for systematic uncertainty analysis.

Topological cuts:
$LdL_{\Xi^-} > 5, (6), 7$
$DCA_{\Lambda-\pi} < 0.7, (0.8), 0.9cm$
$DCA_{p-\pi^-} < 0.6, (0.8), 1cm$
$\chi^2_{prim} > 5, (10), 15$
Track nHitsFit:
nHitsFit>=(15),17,23
raw yield extraction fit region:
$(\pm 10\sigma), \pm 8\sigma, \pm 6\sigma$
Extrapolation to 0 p_T:
(exp m_T), levy, BW, exp p_T

0-10%	nHitsFit	χ^2 primary	Ξ^- LdL	$p-\pi^-$ dca	$\Lambda-\pi^-$ dca	count
$-0.80 < y < -0.60$	10-18%	5-12%	5-9%	4-7%	3-10%	2-3%
$-0.60 < y < -0.40$	2-21%	4-12%	4-9%	1-15%	2-10%	1-5%
$-0.40 < y < -0.20$	1-21%	4-13%	6-10%	2-15%	3-10%	1-5%
$-0.20 < y < 0.00$	3-21%	2-13%	3-10%	2-15%	1-10%	5-12%
10-40%	nHitsFit	χ^2 primary	Ξ^- LdL	$p-\pi^-$ dca	$\Lambda-\pi^-$ dca	count
$-0.80 < y < -0.60$	5-12%	3-14%	5-7%	2-4%	3-7%	1-2%
$-0.60 < y < -0.40$	4-31%	7-28%	3-12%	2-5%	4-14%	1-15%
$-0.40 < y < -0.20$	3-31%	6-28%	3-12%	1-7%	4-14%	2-15%
$-0.20 < y < 0.00$	4-31%	4-28%	3-12%	3-7%	6-14%	6-18%

TABLE III. systematic uncertainty contribution from different cut for m_T spectra, systematic uncertainties varied by p_T bins.

0-10%	nHitsFit	χ^2 primary	Ξ^- LdL	$p - \pi^-$ dca	$\Lambda - \pi^-$ dca	count	fit extrapolation
$-0.80 < y < -0.60$	7%	19%	8%	10%	7%	7%	19%
$-0.60 < y < -0.40$	11%	3%	6%	11%	6%	3%	12%
$-0.40 < y < -0.20$	6%	9%	4%	2%	5%	2%	12%
$-0.20 < y < 0.00$	16%	6%	4%	7%	3%	4%	14%
10-40%	nHitsFit	χ^2 primary	Ξ^- LdL	$p - \pi^-$ dca	$\Lambda - \pi^-$ dca	count	fit extrapolation
$-0.80 < y < -0.60$	4%	16%	7%	4%	1%	2%	13%
$-0.60 < y < -0.40$	22%	7%	3%	3%	5%	13%	16%
$-0.40 < y < -0.20$	7%	7%	2%	2%	6%	3%	15%
$-0.20 < y < 0.00$	14%	4%	3%	4%	11%	24%	14%

TABLE IV. systematic uncertainty contribution from different cut for dN vs. y distribution.

0-10%	nHitsFit	χ^2 primary	Ξ^- LdL	$p - \pi^-$ dca	$\Lambda - \pi^-$ dca	count
$-0.80 < y < -0.60$	2%	7%	6%	4%	2%	2%
$-0.60 < y < -0.40$	2%	1%	1%	3%	1%	1%
$-0.40 < y < -0.20$	3%	3%	2%	1%	1%	0%
$-0.20 < y < 0.00$	5%	3%	1%	2%	1%	2%
10-40%	nHitsFit	χ^2 primary	Ξ^- LdL	$p - \pi^-$ dca	$\Lambda - \pi^-$ dca	count
$-0.80 < y < -0.60$	5%	3%	1%	2%	1%	2%
$-0.60 < y < -0.40$	3%	3%	2%	1%	1%	0%
$-0.40 < y < -0.20$	2%	1%	1%	3%	1%	1%
$-0.20 < y < 0.00$	2%	7%	6%	4%	2%	2%

TABLE V. systematic uncertainty contribution from different cut for T vs. y distribution.

uncertainty contribution from different cut in each rapidity bin.

On the other hand, from the m_{T} exponential function fit of the dN/dp_{T} spectrum, we can extract the fit parameter T. Fig. **??** shows the Ξ^- T vs. y distribution distributions for 0-10% and 10-40% centrality, the line show the statistic uncertainty and the bracket shows the total systematic uncertainty include uncertainties from different topological cuts, raw yield extraction. Tab. **??** lists the relative systematic uncertainty contribution from different cut in each rapidity bin.

By integrating the measured rapidity and using the Gaussian fit to extrapolate, the multiplicities

Centrality	nHitsFit	χ^2 primary	Ξ^- LdL	$p - \pi^-$ dca	$\Lambda - \pi^-$ dca	count	fit extrapolation
0-10%	8%	5%	1%	3%	3%	1%	14%
10-40%	3%	3%	2%	1%	3%	5%	14%

TABLE VI. systematic uncertainty contribution from different cut for total integrated yield production N_{tot}.

Centrality	nHitsFit	χ^2 primary	Ξ^- LdL	$p - \pi^-$ dca	$\Lambda - \pi^-$ dca	count
0-10%	7%	8%	7%	7%	7%	7%
10-40%	5%	6%	5%	5%	5%	5%

TABLE VII. systematic uncertainty contribution from different cut for total integrated yield production T_{eff}.

per triggered event of the Ξ^- can be obtained. Tab. **??** shows the Ξ^- integrated yield production N_{tot} systematic uncertainty for each systematic uncertainty source at $0 - 10\%$ and $10 - 40\%$ centrality, we can see the most largest one is from fit extrapolation.

By fitting the measured dT/dy with $\cosh{(y)}$, the T_{eff} parameters can be obtained. Tab. **??** shows the T_{eff} parameters systematic uncertainty for each systematic uncertainty source at $0 - 10\%$ and $10 - 40\%$ centrality, we can see the most largest one is from fit extrapolation.

For the individual ϕ-meson and Ξ^- measurement, there are two common uncertainties which are correlated or partially correlated: nHitsFit and χ^2 primary(CA for ϕ analysis) cuts. To avoid the correlation in the ϕ/Ξ ratio measurement, we vary the above cuts simultaneous for ϕ and Ξ^-, then quote the final ratio difference directly as the systematic uncertainties. For the other sources, include $n\sigma_k$, $1/\beta$, Ξ^- LdL, $p - \pi^-$ dca, $\Lambda - \pi^-$ dca, Ξ^- raw yield extraction, ϕ and Ξ^- low p_{T} extropolation, those compotents are added quadratic for the ϕ/Ξ^- ratio. Tab. **??** gives the ϕ/Ξ^- ratio systematic uncertainties for each systematic uncertainty source at $0 - 10\%$ and $10 - 40\%$ centrality. For the systematic uncertainties, in general, nHitsFit, χ^2 primary and Ξ^-, ϕ fit extrapolation contributed a lot.

Centrality	nHitsFit	χ^2 primary	$n\sigma_k$	$1/\beta$	Ξ^- LdL	$p - \pi^-$ dca	$\Lambda - \pi^-$ dca	Ξ^- count	Ξ^- extra.	ϕ extra.
0-10%	10%	6%	0%	1%	1%	3%	3%	1%	14%	15%
10-40%	14%	12%	1%	1%	2%	1%	3%	4%	14%	14%

TABLE VIII. The ϕ/Ξ^- ratio systematic uncertainties for each systematic uncertainty source at $0 - 10\%$ and $10 - 40\%$ centrality.

Centrality	$< \Xi > (10^{-3})$	$T_{\text{eff}}(MeV)$	ϕ/Ξ^-
0-10%	$13.87 \pm 0.76 \pm 2.36$	$156 \pm 3 \pm 26$	$1.45 \pm 0.13 \pm 0.34$
10-40%	$3.61 \pm 0.32 \pm 0.59$	$146 \pm 4 \pm 19$	$2.34 \pm 0.23 \pm 0.65$

TABLE IX. Ξ^- integrated yield and T_{eff} as well as ϕ/Ξ^- ratio for given centrality classes in Au+Au collisions at $\sqrt{s_{NN}} = 3$ GeV. The first given error corresponds to the statistical, the second to the systematic error.

The measured Ξ^- in 4π and the extracted T_{eff} parameters as well as ϕ/Ξ^- ratio in different centrality bins are listed in Tab. **??**.

5. RESULTS AND DISCUSSION

Fig. **??** shows the ϕ/Ξ^- ratio as a function of center of mass energy $\sqrt{s_{NN}}$. The colored full symbols show these measurement in two centrality bins, whereas the other data points represented by different markers from various energies and collision system. The red arrow depict the Ξ^- production threshold in NN collisions. The grey solid line represent the calculation from grand canonical ensemble calculation (GCE). The blue band shows transport model calculations from UrQMD.

6. SANITY CHECKS

6.1. Ξ^- spectra symmetry along with rapidity

We have the acceptance with $0 < y < 0.4$, by checking if there is a rapidity symmetry alone 0 for Ξ^- p_T spectrum after efficiency correction, we can test if the Ξ^- reconstruction efficiency is reliable. Fig.**??** shows the Ξ^- efficiency corrected p_T spectra at 0-10%, 10-40%, 0-40% collisions as a function of transverse momentum for two flipped rapidity regions, one is for positive rapidity and another is for negative. We see the positive rapidity p_T spectra is consistent with negative rapidity regions within statistic uncertainty.

Fig.**??** represent efficiency corrected the invariant yield as a function of transverse mass kinetic energy $(m_T - m_0)$ for various rapidity regions in 0–40% centrality. Dashed lines depict exponential function fits to the measured data points. We see the positive rapidity p_T spectra is consistent with

166 negative rapidity regions within total statistic and systematic uncertainty.

6.2. Ξ^- spectra with exclusive eta cut

169 Since the embedding have some discrepancy with the data, we also did this exclusive check
170 like in K^- spectra by removing those $-0.3 < \eta < 0$ ranges tracks and do the systematic checks
171 on the p_T spectra and rapidity distributions. Fig. **??** shows the Ξ^- p_T spectra at 0-10% collisions
172 for the default inclusive one ($\eta < 0$) and exclusive one ($\eta < -0.3$). As can see they are consistent
173 within the rapidity acceptance ranges $-0.8 < y < 0$.

174 Fig. **??** shows the comparison of the rapidity distributions between the default inclusive one
175 ($\eta < 0$) and exclusive one ($\eta < -0.3$). After perform the Gaussian fit, right plot also shows the
176 integrated cross-section values with different colors, the difference is about 3%.

6.3. Ξ^- lifetime

178 To extract the lifetime, we first extract the number of raw counts in different $L/\beta\gamma$ bins, thus
179 obtaining $\Delta N_{raw}/\Delta(L/\beta\gamma)$. We then correct these raw distributions by dividing by the efficiency as
180 a function of $L/\beta\gamma$. The corrected yield is calculated using the formula:

$$\frac{\Delta N}{\Delta(L/\beta\gamma)} = \frac{1}{\varepsilon(L/\beta\gamma)} \times \frac{\Delta N_{raw}}{\Delta(L/\beta\gamma)} \tag{1}$$

181 Finally, an exponential function is fitted to the distribution $\Delta N_{raw}/\Delta(L/\beta\gamma)$ with fit option "I".
182 The measured lifetime is equal to the inverse of the negative slope of the fit divided by the speed
183 of light.

184 We use 5 $L/\beta\gamma$ bins for Ξ [3, 6, 10, 16, 24, 40][cm], the invariant mass distributions for each
186 bin are shown in Fig. **??** at 0-40% collisions.

188 The extracted Ξ raw counts and efficiecny at 0-10%, 10-40%, 0-40% are show in Fig. **??**.

189 The yields can be described by a simple decay law:

$$N(t) = N_0 e^{L/\beta\gamma c\tau} \tag{2}$$

190 where τ is the lifetime and c is the speed of light. Thus, we fit the corrected yield as a function
191 of $L/\beta\gamma$ with a exponential function to extract the lifetime. The fit are shown in Fig. **??**. This is
192 consistent with Ξ lifetime from PDG.

7. APPENDIX

Fig. **??** shows Ξ^- raw yield extraction invariant mass distribution for each rapidity bin at 0-10% collisions.

Fig. **??** shows Ξ^- raw yield extraction invariant mass distribution for each rapidity bin at 10-40% collisions.

chapterZ/fig/drawTopo_nhits.pdf

chapterZ/fig/drawTopo_dca.pdf

chapterZ/fig/xidNdmT_Rotation_EPmethod_fxt3GeV.pdf

chapterZ/fig/xidNdpT_Rotation_EPmethod_fxt3GeV.pdf

chapterZ/fig/xidNdY_Rotation_EPmethod_fxt3GeV.pdf

FIG. 8. Ξ^- reconstruction efficiency before and after weighting, for each p_T-rapidity bins, for $0 - 10\%$(left) and $10 - 40\%$(right) centrality at $\sqrt{s_{NN}} = 3$ GeV.
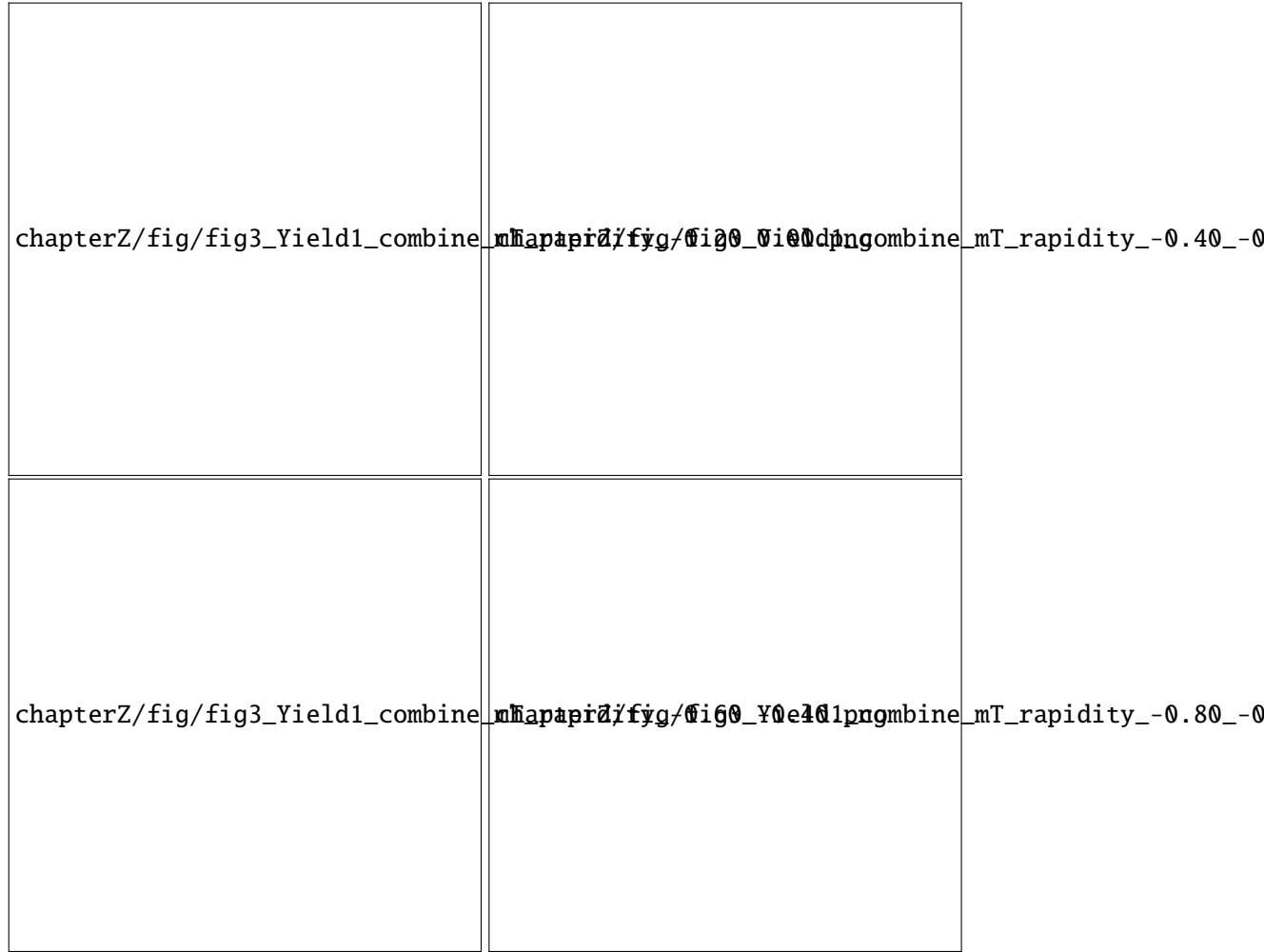
chapterZ/fig/fig3_Yield1_combine_mT_rapidity... chapterZ/fig/fig3_Yield1_combine_mT_rapidity_-0.40_-0...

chapterZ/fig/fig3_Yield1_combine_mT_rapidity... chapterZ/fig/fig3_Yield1_combine_mT_rapidity_-0.80_-0...

FIG. 9. Efficiency corrected Ξ^- m_T spectra comparison for different cuts, for $0-10\%$ and $10-40\%$ centrality at $\sqrt{s_{NN}} = 3$ GeV.

chapterZ/fig/fig55_30 chapterZ/fig/fig55_30 chapterZ/fig/fig55_30 chapterZ/fig/fig55_30

chapterZ/fig/fig55_30 chapterZ/fig/fig55_30 chapterZ/fig/fig55_30 chapterZ/fig/fig55_30
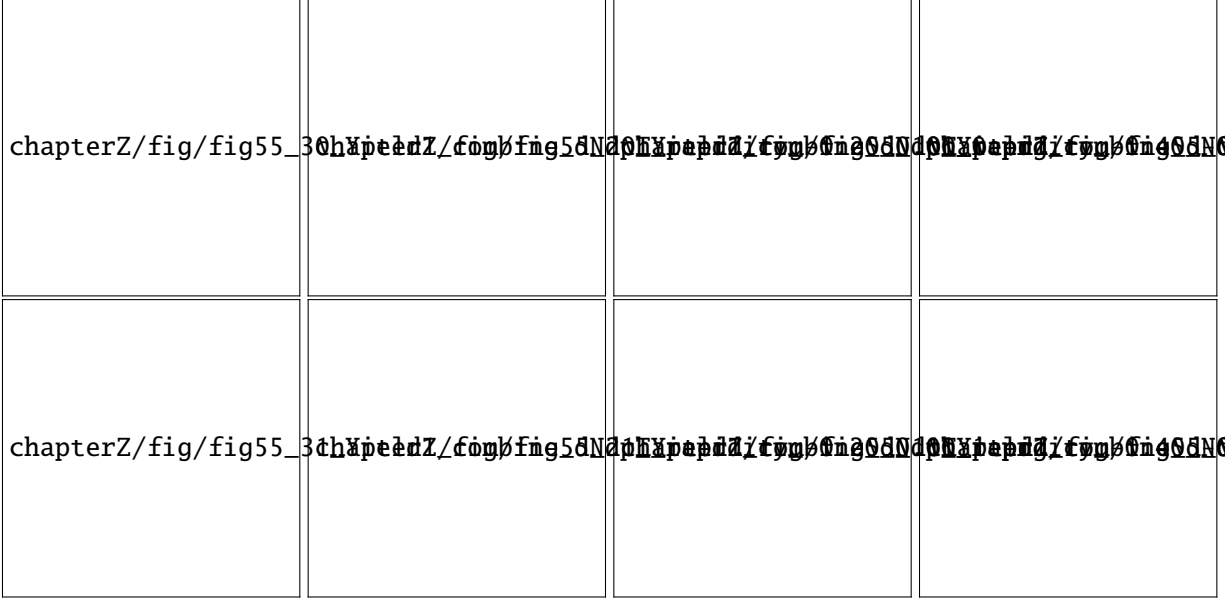
FIG. 10. Efficiency corrected Ξ^- p_T spectra comparison for different function extrapolation, for 0-10%(upper) and 10-40%(bottom) centrality.
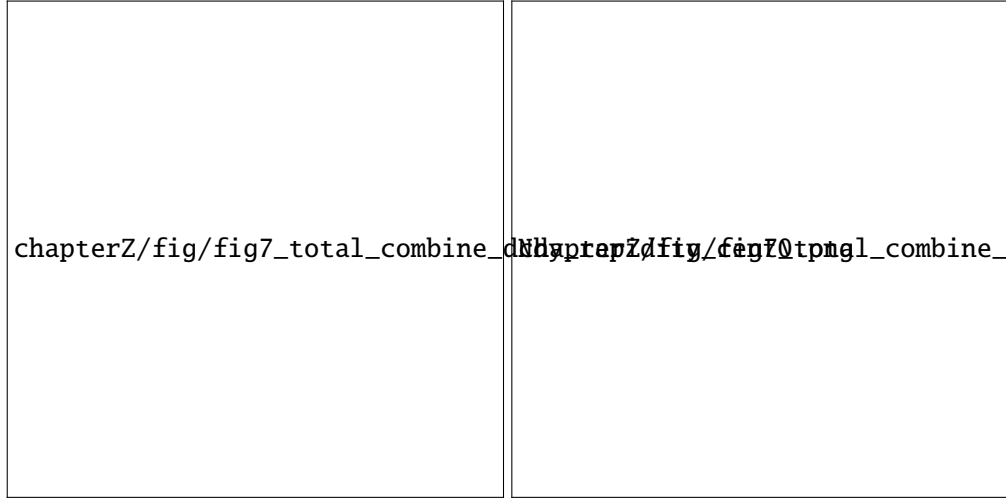
chapterZ/fig/fig7_total_combine_dNdy chapterZ/fig/fig7_total_combine_dNdy_rapidity_cent1.p

FIG. 11. Efficiency corrected Ξ^- dN vs. y distribution, the line show the statistic uncertainty and the bracket shows the total systematic uncertainty

FIG. 12. Efficiency corrected Ξ^- T vs. y distribution, the line show the statistic uncertainty and the bracket shows the total systematic uncertainty
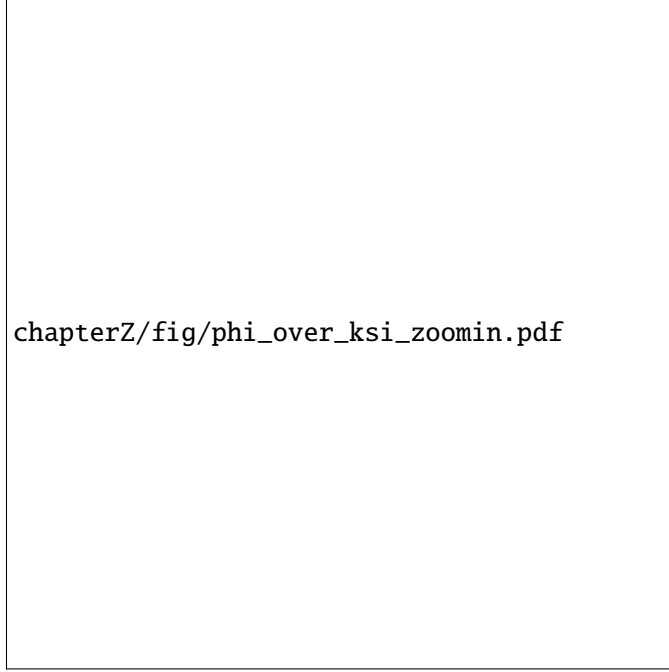
chapterZ/fig/phi_over_ksi_zoomin.pdf

FIG. 13. ϕ/Ξ^- ratio as a function of center of mass energy $\sqrt{s_{NN}}$. The Colored symbols represent two different centralities.

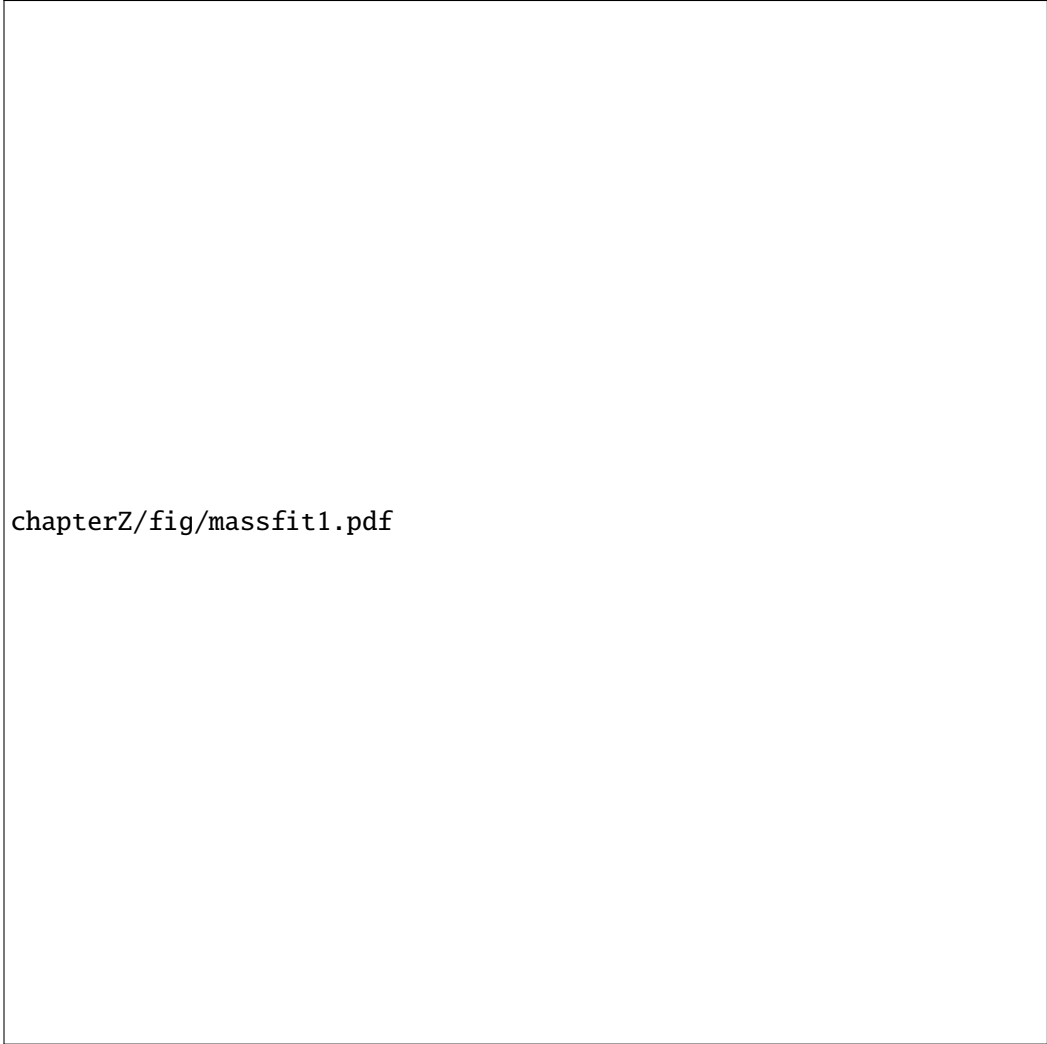chapterZ/fig/xidNdpT_Rotation_EPmethod_fxt3GeV_eta1.pdf

chapterZ/fig/xidNdpT_Rotation_EPmethod_fxt3GeV_eta2.pdf

FIG. 15. Efficiency corrected Ξ^- m_T spectra comparison for different rapiditys, for 0-40% centrality at $\sqrt{s_{NN}} = 3$ GeV.

FIG. 16. Efficiency corrected Ξ^- p_T spectra at 0-10%(upper) and 10-40%(bottom) collisions for the default inclusive one ($\eta < 0$) and exclusive one ($\eta < -0.3$).

FIG. 17. Comparison of the rapidity distributions (upper) and integrated cross-section values (bottom) between the default inclusive one ($\eta < 0$) and exclusive one ($\eta < -0.3$).
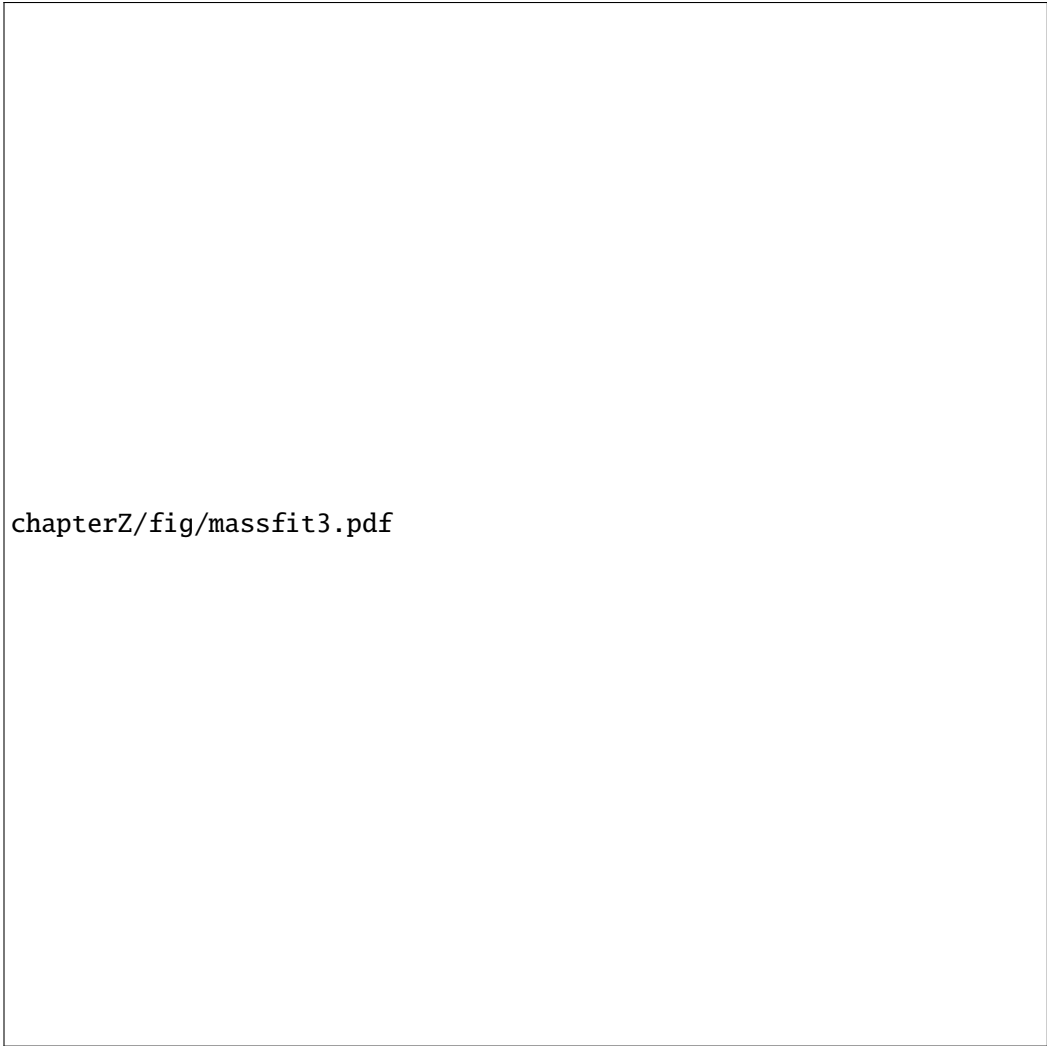
22

chapterZ/fig/massfit1.pdf

chapterZ/fig/massfit2.pdf

FIG. 18. Invariant mass of $\Lambda - \pi^-$ pairs in different $L/\beta\gamma$ bins at 0-40% centrality.

chapterZ/fig/massfit3.pdf

FIG. 19. Extracted raw counts of $\Lambda - \pi^-$ pairs and efficiency as a function of $L/\beta\gamma$ bins at 0-10%, 10-40%, 0-40% centrality.

chapterZ/fig/massfit5.pdf

FIG. 20. Corrected yield as a function of $L/\beta\gamma$ for Ξ at 0-10%, 10-40%, 0-40% centrality.

chapterZ/fig/invMassVsYCent0_dNdYFow_Xi_Rotation_EPmethod_fxt3GeV.pdf

chapterZ/fig/invMassVsYCent0_dNdY0_Xi_Rotation_EPmethod_fxt3GeV.pdf

chapterZ/fig/invMassVsYCent1_dNdYFow_Xi_Rotation_EPmethod_fxt3GeV.pdf

chapterZ/fig/invMassVsYCent1_dNdY0_Xi_Rotation_EPmethod_fxt3GeV.pdf